

Orbital excitations in LaMnO₃ studied by resonant inelastic x-ray scattering

T. Inami, T. Fukuda, and J. Mizuki

*Synchrotron Radiation Research Center, Japan Atomic Energy Research Institute (SPring-8), Hyogo 679-5148, Japan
and Core Research for Evolutional Science and Technology (CREST), Tsukuba 305-0047, Japan*

S. Ishihara

*Department of Physics, Tohoku University, Sendai 980-8578, Japan
and Core Research for Evolutional Science and Technology (CREST), Tsukuba 305-0047, Japan*

H. Kondo

*Institute for Materials Research, Tohoku University, Sendai 980-8577, Japan
and Core Research for Evolutional Science and Technology (CREST), Tsukuba 305-0047, Japan*

H. Nakao, T. Matsumura, K. Hirota, and Y. Murakami

*Department of Physics, Tohoku University, Sendai 980-8578, Japan
and Core Research for Evolutional Science and Technology (CREST), Tsukuba 305-0047, Japan*

S. Maekawa and Y. Endoh

*Institute for Materials Research, Tohoku University, Sendai 980-8577, Japan
and Core Research for Evolutional Science and Technology (CREST), Tsukuba 305-0047, Japan*

(Received 13 September 2002; published 27 January 2003)

We report resonant inelastic x-ray scattering experiments of the orbitally ordered manganite LaMnO₃. When incident photon energy is tuned near the Mn *K* absorption edge, the spectra reveal three features at 2.5, 8, and 11 eV. The 8- and 11-eV peaks are ascribed to transitions from the O 2*p* bands to the empty Mn 3*d* and 4*s*/4*p* bands, respectively. On the other hand, the 2.5-eV peak is considered an orbital excitation across the Mott gap, i.e., an electron excitation from the effective lower Hubbard band with the $d_{3x^2-r^2}$ and $d_{3y^2-r^2}$ orbital characters to the upper Hubbard band with the $d_{y^2-x^2}$ and $d_{z^2-x^2}$ ones. The weak dispersion and characteristic azimuthal angle dependence of this excitation are well reproduced by a theory which includes orbital degeneracy and strong electron correlation.

DOI: 10.1103/PhysRevB.67.045108

PACS number(s): 71.20.-b, 61.10.-i, 71.27.+a, 75.47.Gk

I. INTRODUCTION

The interplay of three degrees of freedom of an electron, i.e., spin, charge, and orbital is now a central issue of the perovskite-type manganites showing the colossal magnetoresistance (CMR) which should be potential functional metallic materials in the next generation.¹ The CMR progenitor LaMnO₃ is a Mott insulator where the electronic configuration of the Mn³⁺ ions is $t_{2g}^3 e_g^1$ with spin quantum number $S=2$. A band gap appears between two e_g bands of the Mn ions hybridized with the O 2*p* orbitals. The occupied e_g orbitals of $3d_{3x^2-r^2}$ and $3d_{3y^2-r^2}$ are alternately ordered in the *ab* plane accompanied by the lattice distortion below 780 K.² With doping of holes in this compound, a variety of electronic phases appear due to the interplay among the multiple degrees of freedom. It is considered, in fact, that the CMR results from the collapse of a subtle balance under the applied magnetic field destroying the orbital ordered state.^{3,4} Most of the previous explorations into this interplay have been directed to spin and lattice dynamics by using various microscopic probes such as neutrons, photons, and electrons.

In contrast, the dynamics of the orbital degree of freedom has not been intensively investigated so far. In orbitally ordered insulators, the dynamics of the orbital is classified into two different excitations. One is a collective orbital excitation termed an orbital wave, which corresponds to the spin

wave in magnetically ordered materials. This orbital wave was recently observed in the Raman-scattering experiments in LaMnO₃ at 120–160 meV at zero momentum transfer.⁵ The other is individual orbital excitation, i.e., the particle-hole excitation, which is related to the Stoner excitations in ordered magnetic systems. In orbitally ordered insulators, the highest occupied and lowest unoccupied electronic states have different orbital characters. Thus a particle-hole excitation across the Mott gap changes the symmetry of the electronic cloud; this is the latter orbital excitation. In this paper, we direct our attentions to this individual orbital excitation. It is well known that the virtual orbital excitation between nearest-neighbor transition-metal ions brings about ferromagnetic superexchange interactions in insulators with alternately ordered orbitals.^{6,7} The observed planar ferromagnetic spin alignment in LaMnO₃ signifies that orbital excitation dominates low-energy electron dynamics. Knowledge of orbital excitations is essential to understand the physics of manganites. Unfortunately, the orbital has no direct coupling to most of experimental probes. Therefore the nature of orbital dynamics in a wide range of energy and momentum remains to be uncovered, unlike spin and lattice dynamics.

In this paper, we report on an investigation of orbital dynamics by means of resonant inelastic x-ray scattering (RIXS) in the hard x-ray regime. This spectroscopy measures

electron dynamics up to a few ten eV as optical conductivity and soft x-ray resonant inelastic scattering observe, but has the advantage of momentum resolution and bulk sensitivity. The resonance enhancement in inelastic x-ray scattering at K -edge was first found in NiO by Kao *et al.*,⁸ and then this technique was applied to recent examinations of electron dynamics in parent compounds of high- T_c superconducting cuprates.^{9–14} In these studies, charge-transfer-type excitations at 6 eV and excitations across a Mott gap ranging a few eV which have a distinct dispersion are reported. Here, RIXS is applied to the CMR progenitor LaMnO_3 . At Mn K absorption edge, we observed a peak at around the energy transfer 2.5 eV in the orbitally ordered state, and measured incident-energy, momentum, and polarization dependence of the peak. We also present a theory of RIXS from orbital excitations. We found that theoretically predicted momentum and polarization dependence of orbital excitations is consistent with the observed results. This leads to a conclusion that RIXS can actually observe orbital dynamics.

II. EXPERIMENT

The experiments were carried out at beam line BL11XU of SPring-8. An inelastic x-ray scattering spectrometer was newly installed in this beamline particularly for RIXS experiments.¹⁵ Incident x rays from a SPring-8 standard undulator were monochromatized by a double-crystal diamond (111) monochromator, and were focused onto a sample by a horizontally bent mirror. The photon flux and the typical spot size at the sample position were about 2×10^{12} photons/sec and 0.12 mm (H) \times 1.4 mm (V), respectively. The horizontally scattered photons were collected by a spherically bent ($R=2$ m) Ge (531) crystal of diameter 76 mm. The total energy resolution, determined from the quasielastic scattering from the sample, was about 0.5 eV full width at half maximum (FWHM). Two single crystals of LaMnO_3 cut from the same boule were used. One has a [110] direction normal to the surface ($Pbnm$ setting). The other consists of two domains due to twinning, and has a and b axes normal to the surface. All data were taken at room temperature.

III. RESULTS

Inelastic scattering is plotted in Fig. 1 as a function of energy loss for several incident energies (E_i) across the Mn K absorption edge ($=6.553$ keV). The resonant nature of the scattering is obvious. Well above and below the absorption edge (spectra a and e), no feature is observed except the elastic scattering at zero energy transfer. The scattering is observed only when the incident energy is close to the absorption edge. The salient spectral features are three peaks at 2.5, 8, and 11 eV, as seen in spectrum c. Note that the resonant energies of the peaks are different from each other. Only the excitation at 2.5 eV is observed in spectrum d, in addition to the broad scattering of the Mn $K\beta_5$ emission line ($3d \rightarrow 1s$). On the other hand, the 2.5-eV peak vanishes in spectrum b, while the 8- and 11-eV peaks remain. This implies different origins of these three peaks.

The momentum (q) dependence of the inelastic scattering

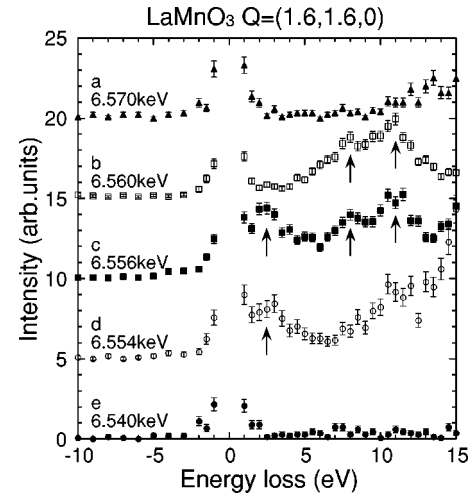


FIG. 1. Inelastic x-ray scattering spectra of LaMnO_3 at $\vec{q} = (1.6, 1.6, 0)$ for five incident energies near the Mn K edge. Data are vertically offset for clarity. Three features at 2.5, 8, and 11 eV are shown by arrows.

along $\vec{q} = (h, h, 0)$ and $(h, 0, 0)$ is shown in Figs. 2(a) and (b), respectively. Three peaks centered at 2.5, 8, and 11 eV seem to show rather flat dispersion. Utilizing the fact that the resonant energy of the 2.5-eV peak differs from that of the 8- and 11-eV peaks, we extracted the 2.5-eV peaks by subtracting data obtained at higher incident energies ($\cong 6.560$ keV) from those obtained at lower incident energies ($\cong 6.556$ keV), and fitted them using a Lorentzian curve. The energy width was fixed in the fitting. The peak position of the 2.5-eV peak obtained is plotted in Figs. 2(c) and (d). The energy disper-

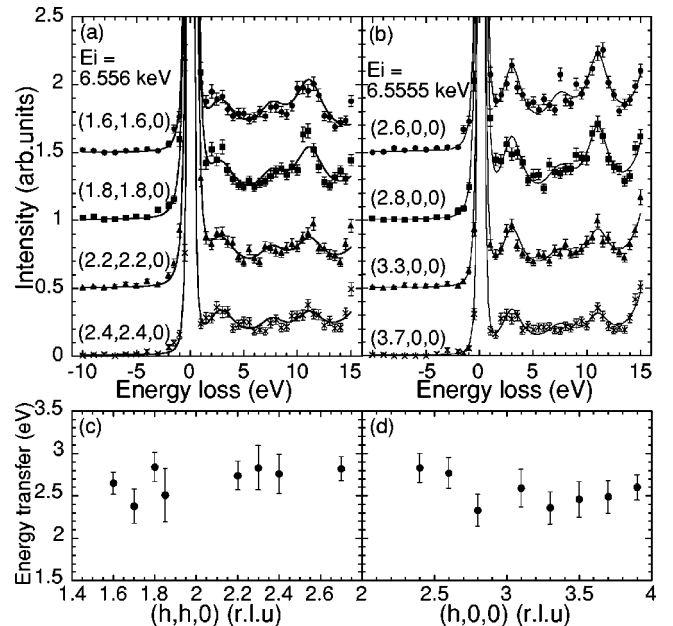


FIG. 2. q dependence of the resonant x-ray scattering spectra along $\vec{q} = (h, h, 0)$ (a) and $\vec{q} = (h, 0, 0)$ (b) at incident photon energies 6.556 and 6.555 keV, respectively. Data are offset for clarity. Solid lines are guides to the eye. The peak positions of the 2.5-eV peak obtained from the fitting are also shown [(c) and (d)].

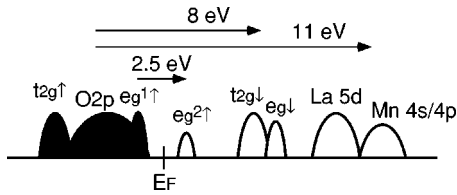


FIG. 3. A schematic band diagram of LaMnO_3 proposed by optical conductivity and photoemission studies. The solid and open areas represent valence and conduction bands, respectively. $e_g^1\uparrow$ and $e_g^2\uparrow$ are states in which the two e_g orbitals are singly and doubly occupied by (an) electron(s) of up spin, respectively.

sion of the 2.5-eV peak is less than a few hundred meV. We also fitted data measured at $E_i=6.560$ keV along $\vec{q}=(h,h,0)$ for the 8- and 11-eV peaks. The data were well reproduced by two Lorentzian curves with q independent peak position and linewidth. The intensity of the 8-eV peak shows weak q dependence, while the intensity of the 11-eV peak largely decreases as q is increased.

Assignments of these peaks are made with the aid of a band diagram estimated in optical conductivity and photoemission measurements, which is depicted in Fig. 3.^{16–19} Optical conductivity measurements revealed that a broad peak exists around 10 eV, which is ascribed to several transitions, such as $\text{O } 2p \rightarrow \text{Mn } 3d$, $\text{La } 5d$, and $\text{Mn } 4s/4p$.^{16–18} The 8- and 11-eV peaks should be included in these transitions, and the resonant nature of the 8- and 11-eV peaks indicates that Mn bands take part in both of the transitions. Accordingly, we ascribed the 8- and 11-eV peaks to transitions from $\text{O } 2p$ to empty Mn $3d$ and Mn $4s/4p$ bands, respectively. The weak q dependence of the 8- and 11-eV peaks in peak position is consistent with the characteristic of local excitations.

On the other hand, the 2.5-eV peak is considered to be a transition from the effective lower Hubbard band (LHB: $\text{O } 2p + e_g^1\uparrow$) to the upper Hubbard band (UHB: $e_g^2\uparrow$) across the Mott gap. This is the lowest excitation in LaMnO_3 and the corresponding excitation at zero-momentum transfer is observed in optical conductivity spectra as a definite peak around 2 eV.^{16–18} As mentioned in Sec. I, this excitation is regarded as an orbital excitation. LaMnO_3 shows the $3d_{3x^2-r^2}/3d_{3y^2-r^2}$ -type orbital order. Since the Mn^{3+} ion has d^4 ($t_{2g}^3 e_g^1$) configuration, one of the two e_g orbitals is occupied by an electron. In the orbitally ordered state, the occupied orbitals are $3d_{3x^2-r^2}$ and $3d_{3y^2-r^2}$ ones. Wannier functions with the e_g symmetry, consisting of oxygen $2p$ orbitals in surrounding oxygen ions, strongly hybridize with these $3d$ orbitals. As a result, the $3d_{3x^2-r^2}$ and $3d_{3y^2-r^2}$ orbitals and the oxygen $2p$ ones with the same symmetries constitute the highest occupied e_g band (LHB). In contrast, the lowest unoccupied e_g band (UHB) consists of the $3d_{y^2-z^2}$ and $3d_{z^2-x^2}$ orbitals which has different orbital symmetry from that of LHB. The excitations from the LHB to the UHB change the symmetry of the orbitals. It is worth mentioning that, in contrast to the present case, in the high- T_c cuprates, both LHB and UHB consist of $3d_{x^2-y^2}$ orbitals. The electronic excitations from LHB to UHB in the cuprates¹² do not change the symmetry of the orbital.

One of the pronounced features of RIXS is polarization

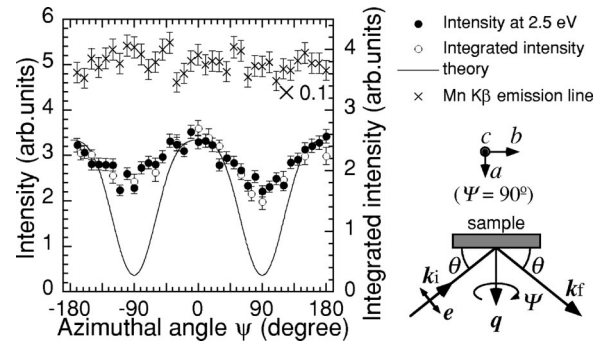


FIG. 4. Azimuthal angle (ψ) dependence of the intensity of the 2.5-eV peak at $\vec{q}=(3.4,0,0)$. Open and solid circles show the integrated intensity of the 2.5-eV peak and the intensity at the energy transfer 2.5 eV, respectively. A solid line shows the integrated intensity of the theoretically calculated RIXS spectra for the orbital ordered LaMnO_3 as a function of ψ . The intensity is scaled so that the maxima approximately agree with the experimental data. Crosses indicate azimuthal angle dependence of the intensity of the Mn $K\beta_5$ emission line at $\vec{q}=(3.4,0,0)$. $E_i=6.555$ keV and $E_f=6.5355$ keV. The intensity is independent of ψ . The experimental setup for the azimuthal angle dependence measurement is also shown. The crystal is rotated about the scattering vector. θ was about 34° . At $\psi=90^\circ$ and 0° , the c axis is perpendicular to and in the scattering plane, respectively.

dependence. Nonresonant inelastic x-ray scattering is not affected by the polarization of the x rays. We measured the polarization dependence of RIXS spectra by changing the azimuthal angle, which is the rotation of the sample about the scattering vector \vec{q} , using the experimental setup shown in Fig. 4. The polarization of the incident photon is in the scattering plane. When the c axis is perpendicular to the scattering plane, the azimuthal angle ψ is defined as 90° . The integrated intensity of the 2.5-eV peak at $\vec{q}=(3.4,0,0)$ is shown in Fig. 4 (open circles) as a function of the azimuthal angle ψ . The 2.5-eV peak was extracted by subtracting an inelastic spectrum measured at $E_i=6.560$ keV from that measured at $E_i=6.5555$ keV, and was fitted by a Lorentzian curve. The peak position and the width were fixed at 2.4 and 3.0 eV (FWHM), respectively, in the fitting. The intensity at the energy transfer 2.5 eV at $\vec{q}=(3.4,0,0)$ is also shown by solid circles. Both intensities exhibit a characteristic oscillation with a twofold symmetry and take their maxima at $\psi=0^\circ$ and 180° . A similar azimuthal angle dependence was observed for the 8- and 11-eV peaks as well. We also measured the Mn $K\beta_5$ fluorescence line, the intensity of which is independent of the azimuthal angle (Fig. 4). This result illustrates that the observed azimuthal angle dependence does not arise from extrinsic origins, such as anisotropic absorption. It also should be emphasized that the azimuthal angle dependence of the 2.5-eV peak is not caused by the shift of resonant energy. If resonant energy at $\psi=90^\circ$ is different from that at $\psi=0^\circ$, oscillation of the scattered intensity at a certain incident energy similar to the observed results is expected. Actually, this is observed in Nd_2CuO_4 , in which the polarization dependence of the RIXS spectra is caused by the 10-eV shift of the resonant energy as a function of the inci-

dent polarization. However, in LaMnO₃, no significant change was observed in the resonant energy of the 2.5-eV peak at $\psi=0$ and 90° . The origin of the azimuthal-angle dependence is therefore completely different from the case of Nd₂CuO₄. The mechanism is discussed in the next section.

IV. THEORY

In this section, we introduce a theory of RIXS from the orbital excitations and compare the calculated results with the experimental results. Consider the scattering of the incident x rays with momentum \vec{k}_i , energy ω_i , and polarization λ_i to \vec{k}_f , ω_f , and λ_f . We start with the conventional expression of the differential scattering cross section given by

$$\frac{d^2\sigma}{d\Omega d\omega_f} = \sigma_e \frac{\omega_f}{\omega_i} \sum_f |S|^2 \delta(\varepsilon_f + \omega_f - \varepsilon_i - \omega_i), \quad (1)$$

where

$$S = \sum_m \left\{ \frac{\langle f | \vec{j}_{-k_i} \cdot \vec{e}_{k_i \lambda_i} | m \rangle \langle m | \vec{j}_{k_f} \cdot \vec{e}_{k_f \lambda_f} | i \rangle}{\varepsilon_i - \varepsilon_m - \omega_f} + \frac{\langle f | \vec{j}_{k_f} \cdot \vec{e}_{k_f \lambda_f} | m \rangle \langle m | \vec{j}_{-k_i} \cdot \vec{e}_{k_i \lambda_i} | i \rangle}{\varepsilon_i - \varepsilon_m + \omega_i + i\Gamma} \right\}, \quad (2)$$

and $\sigma_e = (e^2/mc^2)^2$. $\vec{e}_{k\lambda}$ is the polarization vector of the x ray, Γ is the damping of a core hole, and \vec{j}_k is the current operator corresponding to the transition between Mn 1s and 4p orbitals. The scattering cross section is reformulated by the Liouville operator method. The final form is given by^{19,20}

$$\frac{d^2\sigma}{d\Omega d\omega_f} = \sigma_e \frac{\omega_f}{\omega_i} \sum_{\gamma\gamma'\sigma\sigma'} P_{\gamma\gamma'\sigma\sigma'}^{\lambda_f \lambda_i} P_{\gamma\sigma}^{\lambda_f \lambda_i} \Pi(\omega, \vec{K}), \quad (3)$$

with $\omega = \omega_i - \omega_f$ and $\vec{K} = \vec{k}_i - \vec{k}_f$. $P_{\gamma\sigma}^{\lambda_f \lambda_i}$ describes the polarization part given by

$$P_{\gamma\sigma}^{\lambda_f \lambda_i} = \sum_{\alpha=x,y,z} (\vec{e}_{k_f \lambda_f})_\alpha D_{\gamma\sigma\alpha} (\vec{e}_{k_i \lambda_i})_\alpha, \quad (4)$$

and $\Pi(\omega_i - \omega_f, \vec{k}_i - \vec{k}_f)$ is the Fourier transform of the correlation function of the orbital pseudospin operators defined by

$$\Pi(t, \vec{r}_{l'} - \vec{r}_l) = \frac{|B|^4}{m^2} \langle T_{l'\gamma'\sigma'}^x(t) T_{l\gamma\sigma}^x(0) \rangle, \quad (5)$$

where B is the matrix element of the dipole transition: $B = \frac{1}{2} \langle 4p_\alpha | -i\nabla_\alpha | 1s \rangle$. The orbital excitation is represented by the x component of the pseudospin operator $T_{l\gamma\sigma}^x = d_{l-\gamma\sigma}^\dagger d_{l\gamma\sigma}$ where $d_{l\gamma\sigma}$ is the annihilation operator of the d electron at site l with spin σ and orbital γ and $-\gamma$ indicates the counterpart of γ . The factor $D_{\gamma\alpha}$ in Eq. (4) gives the amplitude of the orbital excitations from the $3d_\gamma$ orbital by x ray with polarization α defined by

$$D_{\gamma\sigma\alpha} = \frac{1}{E_{\gamma\sigma\alpha} - \omega_i + i\Gamma} C_{\gamma\alpha} \frac{1}{E_\alpha - \omega_i + i\Gamma}. \quad (6)$$

E_α and $E_{\gamma\sigma\alpha}$ are the excitation energies of the states $|4p_\alpha^1 3d_{\gamma\sigma} 1s\rangle$ and $|4p_\alpha^1 3d_{-\gamma\sigma} 1s\rangle$, respectively, where $1s$ indicates the state where a hole occupies the $1s$ orbital. We consider that the orbital excitation is caused by the Coulomb interaction between the excited $4p_\alpha$ electron and the $3d_\gamma$ electrons at the same site and its amplitude is represented by $C_{\gamma\alpha}$. The correlation function of the pseudospin operators $\langle T_{l'\gamma'\sigma'}^x(t) T_{l\gamma\sigma}^x(0) \rangle$ is calculated by the generalized Hubbard model with orbital degeneracy using the Hartree-Fock approximation. It is known that, in this approximation, the individual electronic excitations from the lower Hubbard band to the upper Hubbard band, which is our present interest, are emphasized, in comparison with the collective excitations, i.e., orbiton. The Jahn-Teller-type lattice distortion is introduced in the model and the adiabatic approximation is adopted. This is because the RIXS process is faster than the lattice relaxation time. A detailed formulation is presented in Ref. 20.

The obtained RIXS spectra show a gap about $4t$ and a broad peak centered around $6t$, where t is the hopping integral between the nearest-neighboring $3d_{3z^2-r^2}$ orbitals in the z direction and is about 0.5–0.7 eV. The calculated spectra are fitted by a Lorentzian curve. The dispersion of the center of the curve exhibits a weak momentum dependence within $0.1t$. This almost flat dispersion is attributed to the effects of orbital order; the RIXS spectra are approximately given by the convolution of LHB with the $3d_{3x^2-r^2}$ and $3d_{3y^2-r^2}$ orbital characters and UHB with the $3d_{y^2-z^2}$ and $3d_{z^2-x^2}$ ones. Since the electron hopping between the unoccupied orbitals is forbidden in the ab plane, the dispersion of UHB is almost flat (see Fig. 5). As a result, the density of state of LHB dominates the RIXS spectra. This characteristic of the theory based on the orbital excitations is consistent with the results of the experiment shown in Fig. 2.

We obtain the azimuthal angle dependence based on the calculated RIXS spectra. In the actual experimental arrangements shown in Fig. 4, the azimuthal angle dependence of the cross section is given by Eq. (3) where $P_{\gamma\sigma}^{\lambda_f \lambda_i}$ defined in Eq. (4) is replaced by

$$P_{\gamma\sigma}^{\lambda_f \lambda_i} = \sum_{\alpha\beta} (\vec{e}_{k_f \lambda_f})_\alpha (UVD_{\gamma\sigma} V^{-1} U^{-1})_{\alpha\beta} (\vec{e}_{k_i \lambda_i})_\beta. \quad (7)$$

V is a 3×3 matrix describing the transformation from the crystallographic coordinate to the laboratory one, and U is a matrix for the azimuthal angle rotation defined by

$$U = \begin{pmatrix} \cos \psi & -\sin \psi & 0 \\ \sin \psi & \cos \psi & 0 \\ 0 & 0 & 1 \end{pmatrix}, \quad (8)$$

with the azimuthal angle ψ . The polarization vectors are given by

$$\vec{e}_{k_i \sigma_i} = \vec{e}_{k_f \sigma_f} = (1 \ 0 \ 0), \quad (9)$$

$$\vec{e}_{k_i \pi_i} = (0 \ \sin \theta \ \cos \theta), \quad (10)$$

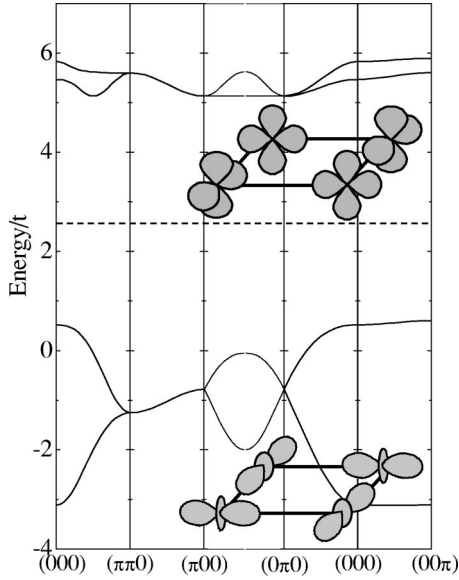


FIG. 5. The electronic band structure for the orbital ordered LaMnO₃. The Hartree-Fock approximation is applied to the generalized Hubbard model where the two e_g orbitals and intrasite Coulomb interactions are taken into account. The alternate ordering of the $3d_{3x^2-r^2}$ and $3d_{3y^2-r^2}$ orbitals in the ab plane is assumed. Broken line indicates the chemical potential located at the center of the highest occupied and lowest unoccupied bands. t is about 0.5–0.7 eV. The inset shows a schematic illustration of the orbital ordered state; the $3d_{y^2-z^2}$ and $3d_{z^2-x^2}$ orbitals (top) constituting the upper Hubbard band and the $3d_{3x^2-r^2}$ and $3d_{3y^2-r^2}$ orbitals (bottom) constituting the lower Hubbard band.

and

$$\vec{e}_{k_f \pi_f} = (0 - \sin \theta \cos \theta), \quad (11)$$

with the scattering angle θ in the laboratory coordinate. The calculated results of the azimuthal angle dependence of the energy-integrated RIXS intensity are shown in Fig. 4 by a solid line. The initial polarization of x rays is chosen to be π and the scattered polarization is summed up for π and σ , since polarization analysis for the scattered x rays were not carried out in the present experiments. Then, we plot $\int d\omega [I_{\pi \rightarrow \pi}(\omega) + I_{\pi \rightarrow \sigma}(\omega)]$ where $I_{\lambda_i \rightarrow \lambda_f}(\omega)$ indicates the differential cross section divided by $(\sigma_e |B|^4 \omega_f) / (4m^2 \omega_i)$. The intensity shows an oscillation with a periodicity $\pi/2$ and becomes minimum (maximum) at $\psi = \pm \pi/2$ (0 and π). When we assume that the polarization dependence is mainly dominated by the factor $C_{\gamma\sigma\alpha}$ in Eq. (6), for simplicity, the azimuthal angle dependence is explicitly obtained as

$$\sum_{\lambda_f = \pi, \sigma} \left. \frac{d^2 \sigma}{d\Omega d\omega_f} \right|_{\lambda_i = \pi} = \sigma_e C_0^2 \frac{\omega_f}{\omega_i} \{ \cos^2 \theta_\gamma P_+ \Pi_+(\omega, \vec{K}) + \sin^2 \theta_\gamma P_- \Pi_-(\omega, \vec{K}) \}, \quad (12)$$

with

$$\Pi_{\pm}(\omega, \vec{K}) = \Pi_{AA}(\omega, \vec{K}) \pm \cos(\vec{K} \cdot \vec{\delta}) \Pi_{AB}(\omega, \vec{K}), \quad (13)$$

$$P_+ = \left(\frac{3}{2} \sin \psi \cos \psi \sin \theta \right)^2 + \left\{ \frac{1}{2} \left(1 - \frac{3}{2} \cos^2 \psi \right) \sin^2 \theta + \frac{1}{2} \cos^2 \theta \right\}^2, \quad (14)$$

and

$$P_- = \frac{3}{4} \sin^2 \psi \cos^2 \theta. \quad (15)$$

We consider the orbital ordered state with two sublattices denoted by A and B , where the occupied orbitals are represented by $|d_{\theta_\gamma}\rangle = \cos(\theta_\gamma/2) |d_{3z^2-r^2}\rangle \pm \sin(\theta_\gamma/2) |d_{x^2-y^2}\rangle$.

$\Pi_{CD}(\omega, \vec{K})$ is the correlation function of the x component of the orbital pseudospin operators in sublattices C and D , defined by $|B|^4 / m^2 F.T. \langle T_{l' \in C \theta_C}^x(t) T_{l \in D \theta_D}^x(0) \rangle$. $\vec{\delta}$ indicates the nearest-neighboring bond connecting the A and B sublattices, and C_0 is a constant part of $C_{\gamma\alpha}$. It is worth noting that the azimuthal angle dependence of the resonant elastic x-ray scattering (RXS) in LaMnO₃ is governed by the factor P_- in Eq. (15). Due to the factor P_+ , which is unique in the inelastic scattering, the minimum value of the scattering intensity becomes finite and the ψ dependence of the intensity includes the higher harmonic components unlike the RXS case in LaMnO₃. The above characteristics of the theoretical results are qualitatively consistent with the experimental data for the 2.5-eV peak. On the other hand, in the ratio of the oscillation amplitude to the ψ independent component, there exists a quantitative discrepancy between theory and experiments. This may be attributed to the approximation adopted in the calculation; in the mean-field approximation, the orbital fluctuations in the ground state are neglected and the oscillation amplitude due to the orbital ordering is thought to be overestimated.

V. SUMMARY

We carried out a resonant inelastic x-ray scattering study of LaMnO₃. Three resonantly enhanced peaks were observed at 2.5, 8, and 11 eV when the incident photon energy was tuned near the Mn K absorption edge. By comparing the peak positions with a previously proposed band diagram, the 2.5-eV peak is attributed to the transition from effective LHB to UHB across the Mott gap, while the 8- and 11-eV peaks are considered excitations from the O $2p$ bands to the empty Mn $3d$ and $4s/4p$ bands, respectively. We also measured the momentum and polarization dependence of the inelastic peaks. The theoretical calculations which include the static orbital order of the Mn³⁺ ions well reproduced the observed weak dispersion and characteristic polarization dependence of the 2.5-eV peak. This result indicates that the 2.5-eV peak can be described as an orbital excitation.

Through the present experimental study of RIXS combined with the theoretical calculation, we have shown that RIXS is a powerful tool for investigating not only the dynamics of electron charge, but also the dynamics of electrons' other degrees of freedom, that is, spin and orbital. With its ability to probe charge, spin, and orbital phenomena, the RIXS technique will provide new insights into the cooperative behavior of these degrees of freedom in complex transition-metal oxides such as the CMR manganites.

ACKNOWLEDGMENTS

We wish to thank T. Iwazumi and T. Arima for their helpful discussions, and are grateful to P. Abbamonte for making the diced Ge analyzer. This work was supported in part by a Grant-in-Aid for Scientific Research Priority Area from the Ministry of Education, Science, Sport, Culture and Technology of Japan, and Science and Technology Special Coordination Fund for Promoting Science and Technology of Japan.

-
- ¹Y. Tokura and N. Nagaosa, *Science* **288**, 462 (2000).
²Y. Murakami, J. P. Hill, D. Gibbs, M. Blume, I. Koyama, M. Tanaka, H. Kawata, T. Arima, Y. Tokura, K. Hirota, and Y. Endoh, *Phys. Rev. Lett.* **81**, 582 (1998).
³*Physics of Manganites*, edited by T. Kaplan and S. D. Mahanti (Plenum, New York, 1999).
⁴*Colossal Magnetoresistance Oxides*, edited by Y. Tokura (Gordon and Breach, Amsterdam, 2000).
⁵E. Saitoh, S. Okamoto, K. T. Takahashi, K. Tobe, K. Yamamoto, T. Kimura, S. Ishihara, S. Maekawa, and Y. Tokura, *Nature (London)* **410**, 180 (2001).
⁶J. B. Goodenough, *Phys. Rev.* **100**, 564 (1955).
⁷J. Kanamori, *J. Phys. Chem. Solids* **10**, 87 (1959).
⁸C.-C. Kao, W. A. L. Caliebe, J. B. Hastings, and J.-M. Gillet, *Phys. Rev. B* **54**, 16 361 (1996).
⁹J. P. Hill, C.-C. Kao, W. A. L. Caliebe, M. Matsubara, A. Kotani, J. L. Peng, and R. L. Greene, *Phys. Rev. Lett.* **80**, 4967 (1998).
¹⁰P. Abbamonte, C. A. Burns, E. Isaacs, P. M. Platzman, L. L. Miller, S. W. Cheong, and M. V. Klein, *Phys. Rev. Lett.* **83**, 860 (1999).
¹¹K. Hamalainen, J. P. Hill, S. Huotari, C.-C. Kao, L. E. Berman, A. Kotani, T. Ide, J. L. Peng, and R. L. Greene, *Phys. Rev. B* **61**, 1836 (2002).
¹²M. Z. Hasan, E. D. Isaacs, Z.-X. Shen, L. L. Miller, K. Tsutsui, T. Tohyama, and S. Maekawa, *Science* **288**, 1811 (2000).
¹³M. Z. Hasan, P. A. Montano, E. D. Isaacs, Z.-X. Shen, H. Eisaki, S. K. Sinha, Z. Islam, N. Motoyama, and S. Uchida, *Phys. Rev. Lett.* **88**, 177403 (2002).
¹⁴Y. J. Kim, J. P. Hill, C. A. Burns, S. Wakimoto, R. J. Birgeneau, D. Casa, T. Gog, and C. T. Venkataraman, *Phys. Rev. Lett.* **89**, 177003 (2002).
¹⁵T. Inami, T. Fukuda, J. Mizuki, H. Nakao, T. Matsumura, Y. Murakami, K. Hirota, and Y. Endoh, *Nucl. Instrum. Methods Phys. Res. A* **467-468**, 1081 (2001).
¹⁶T. Arima and Y. Tokura, *J. Phys. Soc. Jpn.* **64**, 2488 (1995).
¹⁷Y. Okimoto, T. Katsufuji, T. Ishikawa, T. Arima, and Y. Tokura, *Phys. Rev. B* **55**, 4206 (1997).
¹⁸J. H. Jung, K. H. Kim, D. J. Eom, T. W. Noh, E. J. Choi, J. Yu, Y. S. Kwon, and Y. Chung, *Phys. Rev. B* **55**, 15 489 (1997).
¹⁹T. Saitoh, A. E. Bocquet, T. Mizokawa, H. Namatame, A. Fujimori, M. Abbate, Y. Takeda, and M. Takano, *Phys. Rev. B* **51**, 13 942 (1995).
²⁰H. Kondo, S. Ishihara, and S. Maekawa, *Phys. Rev. B* **64**, 014414 (2001).